Available online at www.sciencedirect.com
SCIENCE DIRECT
ELSEVIER
International Journal of Solids and Structures 43 (2006) 5033–5054
INTERNATIONAL JOURNAL OF SOLIDS and STRUCTURES
www.elsevier.com/locate/ijsolstr

Evaluation of some shear deformable shell elements

A. Laulusa [a], O.A. Bauchau [b,*], J-Y. Choi [b], V.B.C. Tan [c], L. Li [c]

[a] *Simudec (SARL), 62 rue de Fontenay, 94300 Vincennes, France*
[b] *Daniel Guggenheim School of Aerospace Engineering, Georgia Institute of Technology, 270 Ferst Drive, Atlanta, GA 30332-0150, USA*
[c] *Department of Mechanical Engineering, National University of Singapore, 10 Kent Ridge Crescent, Singapore 119260, Singapore*

Received 18 March 2005
Available online 18 October 2005

Abstract

The objective of this paper is to evaluate a number of shell elements. At the same time, a new element is presented that is inspired by the quadrilateral heterosis element, Q8H, and is designated herein as the triangular heterosis element, T6H. Both elements employ the selectively reduced integration method. The elements investigated in this study include *ABAQUS*'s three general-purpose shell elements, *ANSYS*'s six-noded triangular element, T6, and the high-performance MITC9 element available in *ADINA*. The assessment is carried out by subjecting the various elements to several benchmark problems. It is found that for regular meshes, Q8H out-performs other elements and is comparable to MITC9. The performance of T6H is shown to be comparable to that of T6 in most test cases, but superior when very thin shells are considered.

Keywords: Shells; Finite element models; Shear and membrane locking

1. Introduction

Shell structures are widely encountered in many engineering applications and are commonly used in the aerospace, aeronautical and automobile industries. Plate structures are a special case of shell structures because shell theories are a generalization of plate theories. Shell theory is the most difficult amongst structural theories such as curved beam and plate, because it involves a dimensional reduction procedure and must deal with initial curvatures. Shell structures exhibit coupling phenomena that are absent in plates. For example, the well-known membrane–bending coupling is not seen in plate, unless geometrically nonlinear theory is considered and/or anisotropic materials are used. Consequently, shell finite elements are complex compared to other structural elements. A list of references that detail different shell theories and shell elements developed by various groups of researchers can be found in Noor (1990); Noor et al. (1989) and Wempner (1990). Despite their complexities, to forgo the use of shell elements in favor of solid elements would incur substantial

* Corresponding author. Tel.: +1 404 894 0042; fax: +1 404 894 2760.
E-mail address: olivier.bauchau@ae.gatech.edu (O.A. Bauchau).

0020-7683/$ - see front matter © 2005 Elsevier Ltd. All rights reserved.
doi:10.1016/j.ijsolstr.2005.08.006

computational costs for the same level of accuracy. For these reasons, shell elements are still the focus of considerable research, as evidenced by recent publications such as Liu et al. (2000) or Zhang et al. (2000).

In the development of plate and shell elements for general applications, it is necessary to include transverse shear deformations that play an important role for the case of thick plates/shells and thin plate/shells when made of anisotropic materials. In general, transverse shear is accounted for by making use of Mindlin-Reissner plate/shell theory, denoted "first order theory", which involves a constant through-the-thickness transverse shear distribution. High order plate theories also exist; for example, Reddy (1984) presented a plate formulation where the transverse shear distribution through the thickness is quadratic.

It is well known that displacement based Mindlin-Reissner plate/shell elements often exhibit shear locking when elements become thin. For shell elements and curved geometries, membrane locking might also occur. Shear and membrane locking are particularly severe for low-order (linear and quadratic) elements. To overcome shear locking, the following approaches can be used: (a) reduced/selective integration (Zienkiewicz et al., 1971; Pugh et al., 1978; Hughes et al., 1978; Hughes and Liu, 1982), (b) discrete constraints enforcement (Batoz and Lardeur, 1989; Batoz and Katili, 1992), (c) assumed transverse shear strain (McNeal, 1982; Huang and Hinton, 1986; Jang and Pinsky, 1987), (d) mixed interpolation that uses different interpolations for the generalized displacements (displacement and rotation) and transverse shear strain fields (Bathe and Dvorkin, 1986; Bucalem and Bathe, 1993; Chapelle and Bathe, 2003) and (e) anisoparametric interpolation that interpolate the displacement and rotations with different order polynomials (Tessler and Hughes, 1985). Some of these approaches are also used to remedy membrane locking, especially the reduced/selective integration method and the mixed interpolation approach.

A shell element should be applicable to simple plate geometries as well as complex shell geometries for both thick and thin structures. It should provide good accuracy for both displacement and stresses with relatively low cost in terms of CPU time. Finally, it should be sufficiently robust, i.e., should present low sensitivity to element distortion.

In this paper, the performance of several shell elements is reviewed by comparing their predictions in a number of benchmark tests. Among the elements considered are the quadrilateral quadratic heterosis element, Q8H, and the mixed interpolation of tensorial components element, MITC9, developed by Bathe and his coworkers (Bucalem and Bathe, 1993; Chapelle and Bathe, 2003). A new triangular element named T6H derived from the concepts of Q8H is also presented. The paper begins with a short description of the elements investigated. The predictions of the various elements for several benchmark problems are then presented and discussed. Conclusions are offered in the last section of the paper.

2. Presentation and description of the shell elements investigated

Many different shell formulations and elements exist, and it is almost impossible to evaluate them all. In this paper, the performance of selected shell elements is reported and their predictions are compared for a number of benchmark tests. Common shell elements selected for this article include those found in the well-known commercial finite element software package, *ABAQUS*. These are the S4R, S4 and S3R elements. Another element chosen for this report is the six-noded triangle element, denoted T6, found in the commonly used finite element software package, *ANSYS*. Besides these elements, the eight-noded quadrilateral heterosis element, Q8H, the new element mentioned above, T6H, and the mixed interpolation of tensorial components element, MITC9, are also included in this work. The T6 element constitutes a benchmark for the T6H element.

The elements investigated fall into two categories: (I) Q8H, MITC9, T6H, T6 and (II) S3, S4, S3R. The elements in the first group are degenerated three-dimensional (3D) solid elements, whereas those in the second group are based on various shell theories. A description of these elements is given in the following paragraphs.

2.1. Q8H element

Hughes and Cohen (1978) first introduced the quadratic heterosis element Q8H with reduced/selective integration technique for plate bending. For very thin plates, this element is reported to outperform the serendipity element Q8 which uses a uniformly reduced integration rule and presents shear locking for some highly constraint boundary conditions, e.g. clamped conditions. It is also reported that Q8H has convergence

characteristics equivalent to those of the Q9 Lagrange element based on the reduced/selective integration technique, but Q9 might exhibit some artificial mechanism while Q8H does not, see Hughes (1987) and the numerical integration section below. It is interesting to mention, the plate bending element Q8H was shown by Lee and Wong (1982) to be equivalent to an element based on a mixed formulation resulting from the modified Hellinger–Reissner principle. This mixed model element does not have any spurious mechanism. In view of this equivalence, Q8H should not be expected to present monotonic convergence characteristics. For the present work, a Q8H Mindlin shell element was coded based on the degenerated 3D formulation. The detail of this formulation can be found in Zienkiewicz (1977).

2.1.1. Geometry

Consider the shell element depicted in Fig. 1. ξ_1 and ξ_2 are the two curvilinear coordinates lying in the middle plane ω of the shell, and ξ_3 is the coordinate in the thickness direction. The global Cartesian coordinate system (O, x_i) and the associated unit vectors $\mathbf{e}_i$ is also shown.

Fig. 2 illustrates an arbitrary point P on the middle plane ω, the two covariant vectors $a_\alpha(\alpha = 1, 2)$ and the normal unit vector n at P. Fig. 3 shows the side profile of the shell element where Q is an arbitrary point in the

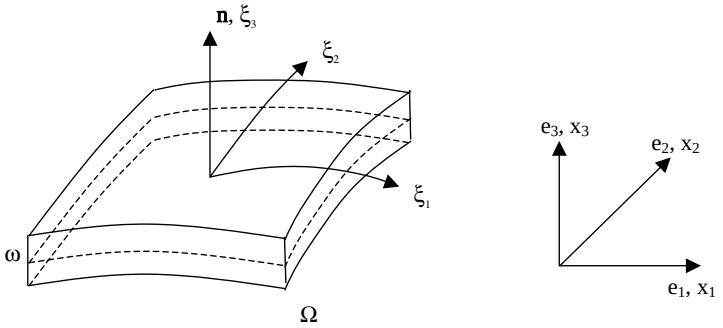

Fig. 1. Curved thick shell element.

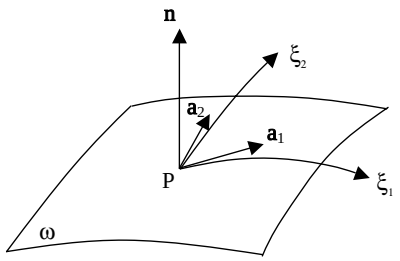

Fig. 2. Mid-plane of thick shell element.

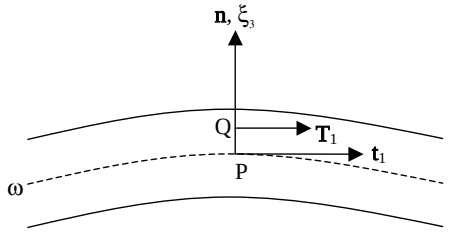

Fig. 3. Cross-section of thick shell element.

thickness direction. t_1 is the unit vector defined from a_1 so that (t_α, n) forms an orthonormal basis at P. Similarly, (T_α, n) constitutes an orthonormal basis at Q.

2.1.2. Discretization

The Q8H shell element considered herein is such that the geometrical terms are discretized using the 8 serendipity interpolation functions. For example, the Cartesian coordinates of $P, x_k^0 (k = 1, 2, 3)$, are

$$x_k^0 = \sum_{i=1}^{n_1} N_i^{(1)} x_{ik}^0 \tag{1}$$

where x_{ik}^0 are the coordinates of node i (Fig. 2); $N_i^{(1)}$ are precisely the serendipity interpolation functions with $n_1 = 8$.

The unit normal vector n is given by

$$\mathbf{n} = \sum_{i=1}^{n_1} N_i^{(1)} \mathbf{n}_i \tag{2}$$

where $\mathbf{n}_i$ are the normal vector at node i.

The position vector OQ is given by

$$\mathbf{OQ} = \sum_{k=1}^{3} \sum_{i=1}^{n_1} N_i^{(1)} x_{ik}^0 \mathbf{e}_k + \frac{\xi_3}{2} \sum_{i=1}^{n_1} N_i^{(1)} h_i \mathbf{n}_i \tag{3}$$

where $h_i = h$ is the constant thickness of the shell element.

The displacement vector $\mathbf{U}$ of the point Q is discretized as,

$$\mathbf{U} = \sum_{k=1}^{3} \sum_{i=1}^{n_1} N_i^{(1)} u_{ik} \mathbf{e}_k + \frac{\xi_3}{2} \sum_{i=1}^{n_2} N_i^{(2)} h_i (\tilde{\theta}_{i2} \mathbf{t}_{i1} - \tilde{\theta}_{i1} \mathbf{t}_{i2}) \tag{4}$$

where u_{ik} are the displacements of node i on the middle plane; $\tilde{\theta}_{i1}, \tilde{\theta}_{i2}$ are the two rotations at node i; $\mathbf{t}_{i1}$, $\mathbf{t}_{i2}$ are the two vectors $\mathbf{t}_1$, $\mathbf{t}_2$ at node i. $N_i^{(2)}$ represent the Lagrange interpolation functions with $n_2 = 9$. In the above equation, ξ_3 varies from -1 to 1.

The heterosis (parent) element is shown in Fig. 4. The external nodes have five degrees of freedom or dofs and the internal node two dofs. The number of dofs of the quadrilateral heterosis element is thus 42.

2.1.3. Numerical integration

The heterosis element uses the selectively reduced integration technique such as that reported in Carnoy and Laschet (1992). This technique generalizes Hughes' segregation method (Hughes and Liu, 1982) to curved shell elements. Bending, membrane and shear strains are separated in the local strain tensor (with respect to the local Cartesian axes) at a point of the shell. The bending part of the stiffness matrix is integrated with a normal integration scheme using nine Gauss points; whereas for the shear and the membrane parts, the four

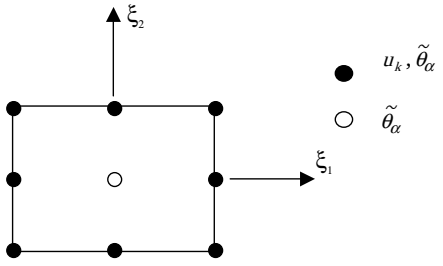

Fig. 4. Parent heterosis element.

Gauss point reduced integration scheme is used. The membrane part is that of the membrane–bending coupling which depends only on the displacements and not the rotations. Two Gauss points are used through the thickness.

2.1.4. Mechanisms

Carnoy and Laschet (1992) reported that the Q8H element based on the selectively reduced integration method possesses one membrane artificial mechanism, which is not communicable, i.e. this zero energy mode does not propagate in a mesh of two or more elements. By analyzing the eigenmodes of the stiffness matrix of a single element, the stiffness matrix was found to exhibit a membrane zero energy mode, in addition to the six legitimate rigid body modes. But when the global stiffness matrix of a mesh of two then four elements is considered, the only zero energy modes found are those of the six rigid body motions, in agreement with Carnoy and Laschet (1992). Although this is not a formal proof of the correct rank of the global stiffness matrix from a mesh featuring an arbitrary number of elements, in practice, the Q8H element "can be viewed as having correct rank" as mentioned by Carnoy and Laschet (1992).

2.2. T6H element

The motivation for developing the T6H is to provide a quadratic triangular element in addition to Q8H to provide flexibility in modeling shell structures. The first author of the present paper developed this element while employed as a consultant by *Electricité de France* (*EDF*). The two elements Q8H and T6H were implemented in the in-house software of *EDF* (Massin et al., 2000), called the *Code_Aster*, which is now in the public domain. This T6H element is inspired by the Q8H element. The seventh internal node has only two dofs as shown in Fig. 5. The number of dofs of this triangular "heterosis" element is thus 32.

For the triangular element, the six functions $N_i^{(1)}$ are those of the quadratic T6 element and the seven functions $N_i^{(2)}$ comprise cubic polynomial resulting from the interpolation function corresponding to internal node of element T10. The seven $N_i^{(2)}$ functions are given in the Appendix.

2.2.1. Discretization

Eqs. (1)–(4) still apply for this element, but here, the functions $N_i^{(1)}$ are Lagrange interpolation functions of the element T6, thus $n_1 = 6$; the functions $N_i^{(2)}$ are cubic polynomials resulting from the shape function corresponding to the internal node of the element T10 with $n_2 = 7$. These seven interpolation functions are given in the Appendix. For this reason, unlike T6, T6H is not a pure quadratic element.

Although T6H uses the concepts of Q8H, the interpolation functions of T6H are not homogeneous as they combine quadratic and cubic polynomials. This scheme, which interpolates the rotations with polynomials of higher degree than those approximating the displacements, is not recommended, in general. Rather, the inverse is recommended to avoid the shear locking; in which case, a normal integration rule can be employed. However, T6H is based on the reduced/selective integration technique, which should alleviate locking.

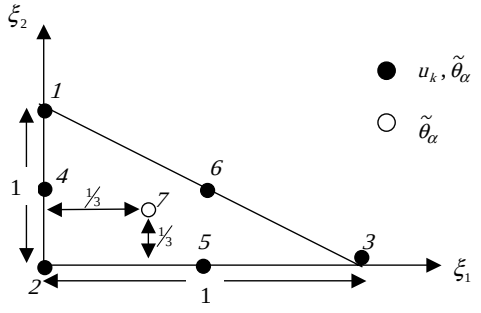

Fig. 5. Parent heterosis triangular element.

2.2.2. Numerical integration

Like the Q8H element, the selectively reduced integration procedure is applied. The bending term is integrated with a normal rule using a seven-point Hammer scheme, whereas both shear and membrane terms (the latter being the membrane–bending coupling which depends only on displacements and not rotations) are integrated with a reduced three-point Hammer scheme. Two Gauss points are used through the thickness.

2.2.3. Mechanisms

To identify the potential artificial mechanisms of the T6H element based on the selectively reduced integration method, the eigen-modes of the stiffness matrix of a single element are analyzed. Interestingly, the results show the sole six legitimate rigid body modes, thus no spurious mechanism has been found. And, not surprisingly, when the global stiffness matrix of a mesh of two elements is investigated, no spurious mechanism is observed. The fact that T6H does not possess any artificial mechanism at the element level is of high importance, as it ensures the correct rank of the global stiffness matrix from a mesh of an arbitrary number of elements.

2.3. T6 element

The next element chosen for this study is the six-noded triangular element found in the SHELL93 library of the finite element software package, *ANSYS*, see ANSYS (1998). It is capable of performing both kinematic and material nonlinear analyses. This element is obtained through the degeneration of the eight-noded Q8 quadrilateral element. This element is selected as a benchmark for the T6H element. The two elements, T6 and T6H, are quite similar, but the formulation of the latter is more complex as it has an internal node. The uniformly reduced integration rule is employed in the T6 element with a three-point Hammer scheme. Two Gauss points are used through the thickness.

The Q8 element is based on a uniformly reduced integration scheme and features two artificial mechanisms, which are not communicable, e.g. see Carnoy and Laschet (1992). As mentioned above, the T6 element is the degenerated version of Q8, and uses a uniformly reduced integration rule. Thus it should also possess artificial mechanisms, but it is unclear whether they are communicable or not.

2.4. S4, S4R and S3 elements

These elements are part of the commercial software *ABAQUS* and are based on a thick shell theory. They serve as general-purpose shell elements in the *ABAQUS* element library. The shell formulation considered is that of finite-membrane strain, therefore, these elements can be used to perform large strain analyses. They are widely used for industrial applications because they are suitable for both thin and thick shells. It is thus useful to compare their performance with that of the other shell elements presented above.

The S4 element uses a normal integration rule with four integration points. The assumed strains approach is employed to prevent shear and membrane locking. The S4R element uses a reduced integration rule with one integration point that makes this element computationally less expensive than S4. For S4R, the assumed strains method is modified, so that a one point integration scheme plus hourglass stabilization is obtained. Hourglass modes, a form of artificial mechanisms, can arise from the use of the reduced integration rule. The hourglass stabilization is performed through an hourglass control parameter. The S3 element is obtained through the degeneration of the S4 element and thus, ''may exhibit overly stiff response in membrane deformation'', as discussed in ABAQUS (1998). The *ABAQUS* shell library also includes the general purpose S3R element. This element is equivalent to S3, yielding identical results to those of S3 for all the problems investigated in this paper. More details can be found about these four elements in ABAQUS (1998).

2.5. MITC9 element

Several shell formulations have been recently developed that have distinguished themselves from other shell formulations because of their versatility, accuracy and robustness. Of particular interest, is the mixed

interpolation of tensorial components (MITC) element developed by Bathe and his coworkers (Bathe and Dvorkin, 1986; Bucalem and Bathe, 1993). The MITC approach is based on the interpolation of strains at chosen sampling points (so-called "tying points"). The key issue of this approach is the selection of the tying points and corresponding interpolation functions. In the present paper, the MITC9 will be used; the interpolated strain components are defined as

$$\varepsilon_{11} = \Sigma_\alpha g^\alpha_{rr}\varepsilon^\alpha_{11}; \quad \varepsilon_{22} = \Sigma_\alpha g^\alpha_{ss}\varepsilon^\alpha_{22}; \quad \varepsilon_{12} = \Sigma_\alpha g^\alpha_{rs}\varepsilon^\alpha_{12} \tag{5a}$$

$$\varepsilon_{13} = \Sigma_\alpha g^\alpha_{rr}\varepsilon^\alpha_{13}; \quad \varepsilon_{23} = \Sigma_\alpha g^\alpha_{ss}\varepsilon^\alpha_{23} \tag{5b}$$

where g^α_{rr}, g^α_{ss} and g^α_{rs} are the strain interpolation functions and ε^α_{ij} the strain components at the α tying point which are obtained by direct interpolation using the finite element displacement assumptions. The location of the tying points and corresponding strain interpolation functions can be found, for example, in Bathe and Dvorkin (1986); Bucalem and Bathe (1993) for each strain components. For the MITC9, the strain components ε_{11} and ε_{13} are interpolated based on six tying points, using the shape functions g^α_{rr}, the strain components ε_{22} and ε_{23} are interpolated based on six tying points, using the shape functions g^α_{ss}, and finally, the in-plane shearing strain components ε_{12} and ε_{13} are interpolated based on four tying points, using the shape functions g^α_{rs}. This approach takes care of both membrane and transverse shearing strain locking problems. The stiffness matrix of the element is then formed based on these interpolated strain components and full integration is used. The element does not present any spurious mechanism. In view of the more complicated strain interpolation and full integration scheme, the MITC9 is a more computationally expensive element, but it is accurate and fairly insensitive to element deformations. The numerical results for MITC9 are those of the *ADINA* program 900 nodes version (ADINA, 2005).

Remark

(1) It is of interest to note that Q8H and T6H are degenerated 3D, rather than isoparametric elements.
(2) Except for MITC9, which features 5 dofs per node (with two rotations), all the elements described above have three rotations per node. The third rotation is the fictitious rotation about the normal and is associated with an artificial small stiffness.

3. Numerical results

The elements described above were exercised on a series of benchmark problems to test their ability to handle different modes of deformation, membrane strains, bending strains or membrane–bending coupling due to initial curvatures, rigid body motion, and to prevent shear and membrane locking. Shear locking can be expected since all the problems considered deal with thin or very thin shells and plates, while membrane locking can also be expected in all the shell problems.

Their performance is to be evaluated in terms of accuracy as a function of the total number of *dof*s, and robustness, i.e. low sensitivity to element distortion. Note that a more rigorous criterion of performance would be CPU time, however, this is quite difficult to establish because the various shells elements were run on different computer systems. As the elements Q8H and T6H have 6 and 3 dofs for external and internal nodes, respectively, the total number of dofs will be taken as a measure of mesh refinement instead of the total number of nodes.

3.1. Scordelis-Lo barrel roof under distributed load

The barrel roof test is a classical benchmark problem that is often used to test membrane locking. Bending strains, although significant, are less important than membrane strains. The geometry of the problem is shown in Fig. 6a. In the present case, angle α subtended by the arc is 80°. The length of the roof is $L = 6$ m; the radius of curvature is $R = 3$ m and its thickness $t = 0.03$ m. The material has a Young's modulus of $E = 30$ GN/m^2 and a Poisson's ratio of $v = 0$. The load it experiences is due to its weight, amounting to the force per unit

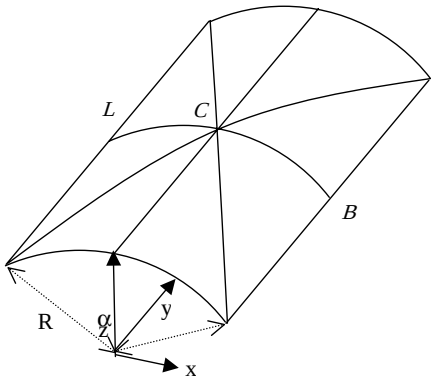

Fig. 6a. The *Scordelis-Lo barrel* roof test – balanced 8-triangular element mesh.

surface $fz = 6250\ \mathrm{N/m^2}$. The two curved edges of the roof are supported by rigid diaphragms while the two straight edges remain free.

Uniform meshes are used for the quadrilateral elements, while the triangular meshes used are arranged as shown in Fig. 6a. This figure illustrates an 8-element mesh, which is obtained from a 2-element per edge mesh for quadrilateral elements. The subsequent refinement of this mesh is a 32-element mesh, obtained with a 4-element per edge mesh for quadrilateral elements, see Fig. 6b for illustration. Such a balanced arrangement, called "English" mesh, as illustrated in Fig. 6a (or Fig. 6b), gives better results than when the triangles are all oriented along the same direction, called biased meshes, as shown in Fig. 6c and 6d. It is worth noting that the meshes for the S3 element are such that the numbers of dofs are identical, but the number of elements is twice that for the S4 and S4R elements. This will be the case as well in the problems that follow. All the elements investigated converge to the deep shell solutions, $W_B = 3.61$ cm and $W_C = 0.541$ cm, which are used to normalize the results.

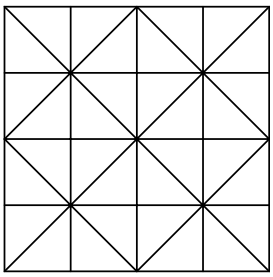

Fig. 6b. Balanced 32-triangular element mesh, for clarity, the initial curvature is not shown.

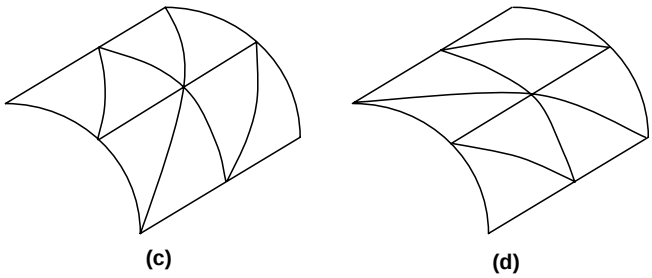

Fig. 6c and 6d. Biased 8-triangular element meshes.

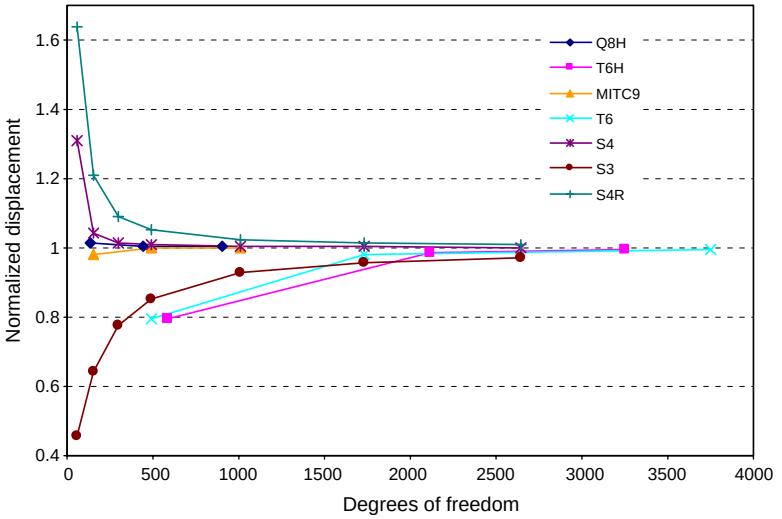

Fig. 7. Normalized displacement of the barrel roof at point C.

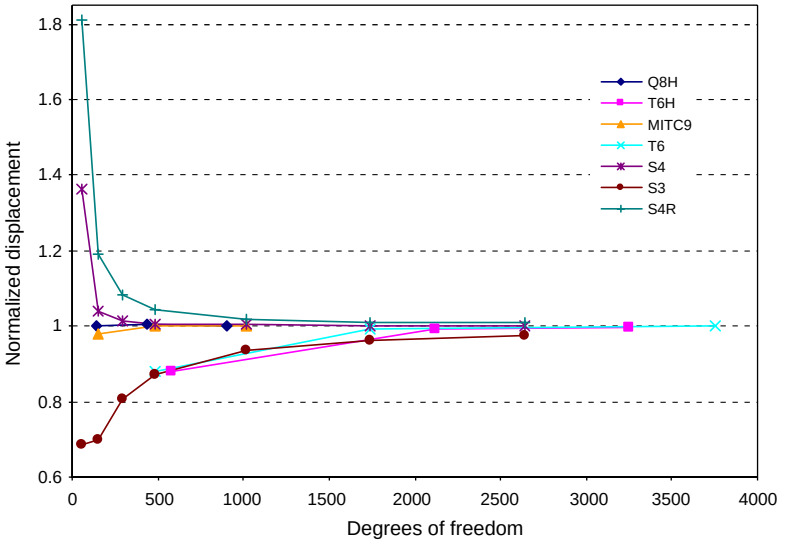

Fig. 8. Normalized displacement of the barrel roof at point B.

As can be observed from Figs. 7 and 8, the Q8H and MITC9 elements exhibit the best performance. Among the *ABAQUS* elements, S4 outperforms S4R as the former evaluates more accurately the membrane strains (ABAQUS, 1998), which constitute the dominant deformation in this example. As expected, S3 shows stiffer response than S4, however, the solutions converge at an acceptable rate. The performances of the T6H and T6 elements are equivalent for this problem and are comparable to that of S3. It is worth noting that the characteristics of monotonic convergence "from below" are no longer guaranteed for the different elements investigated as a pure displacement based finite element using exact integration rule would do. This is illustrated in this example by the Q8H, S4 and S4R elements.

3.2. Pinched cylinder with rigid end diaphragms

A cylinder with rigid end diaphragms is pinched by the application of opposing radial point loads at the top and bottom of the cylinder at the mid-span. The pinched cylinder presents a very severe test case, and

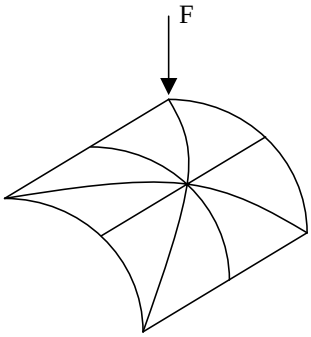

Fig. 9. Geometry and loading of the pinched cylinder test with balanced English mesh.

constitutes a good problem to assess the performance of shell elements. Both membrane and inextensible bending strains are important and so is the membrane–bending coupling. In this problem, the membrane strains field is also known to be complex. Bending is mainly localized near the loading points, and the gradients of the displacements along some edges are important (Batoz and Dhatt, 1992). For this problem, severe membrane locking is expected as bending is inextensible. Due to the three planes of symmetry only one eighth of the cylinder is modeled, as shown in Fig. 9. The remaining edge is left free. The load has a magnitude of $F = 0.25$ N and the length and radius of the cylinder are $L = 300$ m and $R = 300$ m, respectively. The material properties are $E = 3$ MN/m^2 for the Young's modulus and $v = 0.3$ for Poisson's ratio.

Uniform meshes are used for the quadrilateral elements. The triangular meshes used are arranged as shown in Fig. 9 (similar to Fig. 6a). Here again, this balanced ("English") mesh gives better results than when the triangles are all oriented in the same manner (Fig. 6c and 6d). The parameter used for comparing the different elements is the radial displacement under the point of loading. The results are normalized by the reference solution of 1.8248e−5 m, given in Belytschko et al. (1985).

For this severe test, the best performance is obtained with MITC9, and next with Q8H elements, as illustrated in Fig. 10, although convergence is slower than in the previous example. S4R now performs slightly better than S4, the former element should yield better predictions for bending dominant problems, and this is the case near point C. Here again, S3 is stiffer when compared to S4. The performance of T6H is quite similar to that of T6. Both elements converge slowly due to severe membrane locking. For this example, it is interesting to note that all the elements converge monotonically to the reference solution. The results of MITC9 are in excellent agreement with those reported by Bucalem and Bathe (1993).

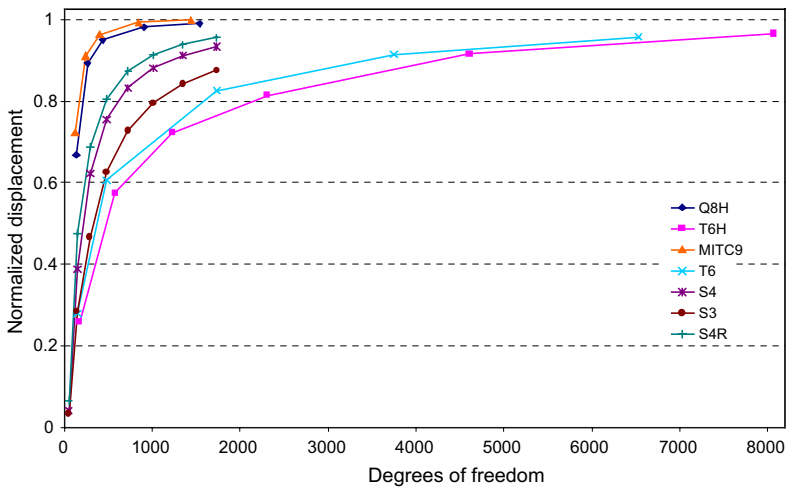

Fig. 10. Displacement of pinched cylinder at point of loading.

3.3. Pinched hemisphere

The pinched hemisphere is another common test problem. This problem is often used to detect severe membrane locking, and test the elements' ability to represent rigid body motions that form a significant component of the total displacement of the structure. The problem comprises a hemispherical dome radially loaded at its equator by two pairs of opposing point loads acting in orthogonal directions. The problem is illustrated in Fig. 11 where only a quarter of the dome is modeled because two orthogonal meridonial planes are planes of symmetry. The top and bottom edges of the hemisphere are unsupported. Unlike the previous test cases, the shell structure is doubly curved. For this problem, bending strains are more important than membrane strains.

For the test case, the radius of the hemisphere is $R = 10$ m and the thickness of the shell is $t = 0.04$ m. The shell has a Young's modulus of $E = 68.25$ MN/m^2 and Poisson's ratio of $v = 0.3$. The top edge of the hemisphere is at latitude of 18°. The point loads applied to the hemisphere have a magnitude of $F = 1$ N. Uniform meshes are used for the quadrilateral elements, while the triangular elements used are balanced, as shown in Fig. 11b. The results obtained for the different shell elements are presented in Fig. 12. The graphs show the radial displacement of the hemisphere at the point of loading normalized by the reference solution of 0.094 m, see McNeal and Harder (1985). Because of symmetry, the magnitudes of the radial displacement at the points of loading should be equal. This is the case when quadrilateral elements are used and when

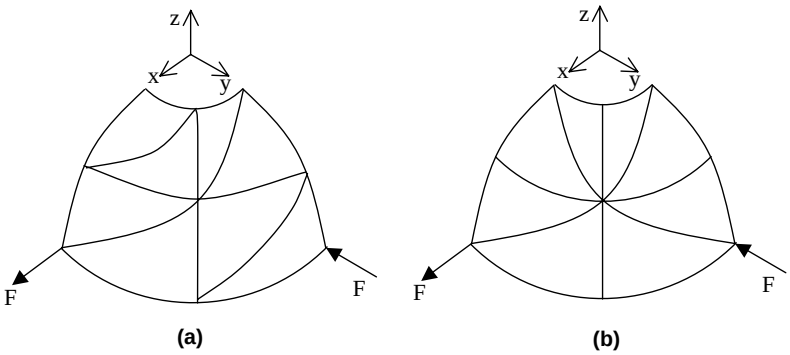

Fig. 11. Geometry and boundary conditions of hemispherical shell test. (a) Biased mesh; (b) Balanced mesh.

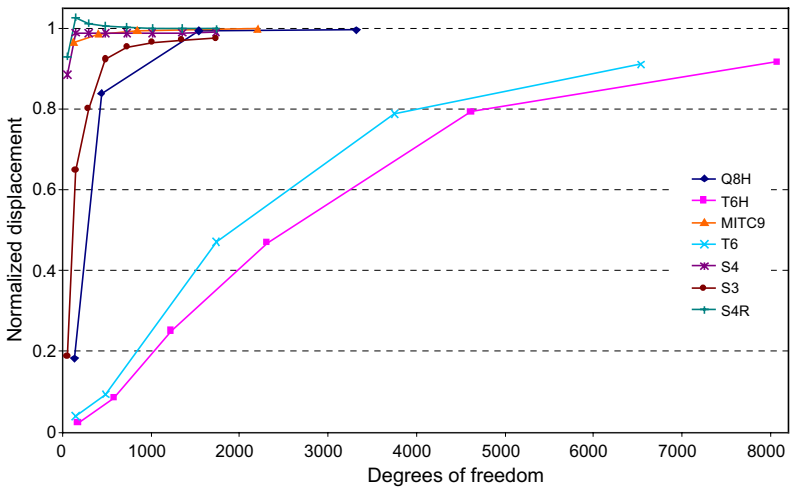

Fig. 12. Displacement of pinched hemisphere at point of loading.

Table 1
Radial displacements at loading points for the T6 element using biased and balanced meshes

Dofs (nodes per edge)	Biased mesh: U_X	Biased mesh: $-U_Y$	Balanced mesh: $U_X = -U_Y$
150 (5)	0.004635	0.004292	0.003737
486 (9)	0.008334	0.007719	0.008856
1734 (17)	0.037311	0.036716	0.044272
3750 (25)	0.069077	0.068410	0.074096
6534 (33)	0.084421	0.082854	0.085653

the triangle elements are balanced, see Fig. 11b. However, when using the biased arrangement of the triangle elements shown in Fig. 11a, the shell becomes more compliant in the x-direction as compared to the y-direction: $|U_X| > |U_Y|$. This phenomenon is illustrated in Table 1 for the T6 element.

The results illustrated in Fig. 12 show that MITC9 then S4R and S4 elements give very good accuracy even with coarse, 2×2 meshes featuring 125 dofs (MITC9) and 54 dofs (S4R and S4). For coarse meshes, these three elements outperform Q8H, which exhibits severe membrane locking for the 2×2 mesh featuring 138 *dof*s. However, very high convergence rate is shown when the mesh is slightly refined, and convergence is reached for Q8H with relatively coarse, 8×8 mesh (1542 dofs). Note that unlike S4R, S4 does not converge to the reference solution for refined meshes; numerical results show an error of about one percent. The S3 element yields good performance as compared to that of T6 and T6H, but here again, inferior to that of S4. The convergence rate of these two elements is slow, denoting persisting membrane locking. The performance of T6 is slightly better than that of T6H. For this problem, also note the monotonic convergence for all the elements except for S4R and S4. The results of MITC9 are in excellent agreement with those reported in Bucalem and Bathe (1993).

3.4. Cantilevered pre-twisted beam

Cantilever pre-twisted beams have become common test problems for shell elements. In this problem, the beam features a large initial twist such that its opposite edges are at a 90° angle with respect to each other. This warping results in bending-membrane coupling. The pre-twisted beam is commonly used to evaluate the ability of quadrilateral elements to handle the double curvature geometries. For very thin beams, this problem will also underline the sensitivity of shell elements to both shear and membrane locking, because the deformation behavior consists of nearly inextensional bending.

The test problem is shown in Fig. 13a. The left horizontal edge is fixed, while the right edge is rotated 90° with respect to the fixed end. Two loading cases are considered: an in-plane shear force P_z and an out-of-plane shear force P_y, as shown in Fig. 13a. The span of the beam is $L = 12$ m and its width $b = 1.1$ m. The problem is solved for two beam thicknesses of $h = 0.32$ m, referred to as "thick beam," in this case the loading is $P_z = P_y = 1$ N, and $h = 3.2$ mm referred to as "very thin beam," in this case the loading is $P_z = P_y = 1\text{e}{-6}$ N. The material has a Young's modulus of $E = 29$ MN/m^2 and Poisson's ratio $v = 0.22$.

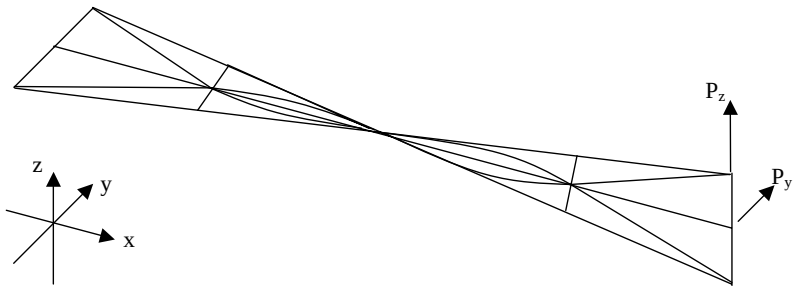

Fig. 13a. Cantilevered pre-twisted beam test.

3.4.1. Thick beam

For Q8H and MITC9, uniform meshes with one element across the width are used, e.g., 1×2, whereas for T6H and T6, the meshes are two elements across the width (2×4) and are arranged as shown in Fig. 13b. An additional balanced mesh with four elements (4×24) across the width is also considered, as shown in Fig. 13a. For S4 and S4R, the meshes have two elements across the width; whereas for S3, there are 4 elements across the width and the meshes are balanced, see Fig. 13a.

Figs. 14 and 15 show the predicted normalized displacements at the tip of the beam with respect to the reference solutions due to out-of-plane loading P_y. The reference solutions are from beam theory: $U_y = 1.75$ and $U_z = -1.72$ mm, see Batoz and Dhatt (1992). For this case, the deformation near the clamped end largely consists of membrane strains. The best performances are obtained with MITC9 and Q8H elements. The curved shell element S4 also yields very good results: its four nodes are not coplanar, a key to the proper handling of the double curvature geometry of the problem. A flat shell element would yield very erroneous predictions, as reported by Batoz and Dhatt (1992). The very stiff results exhibited by S3 as compared to those of S4 are not surprising (Fig. 14), since the membrane strains are important for this loading case. Significant discrepancies compared to the reference solutions are observed for the S4R element as well. The performances of T6H and T6 are fair and comparable to each other.

Fig. 16 shows the results of in-plane loading P_z (reference solution $U_z = 5.42$ mm). For this case, the dominant deformation is bending strain, although some membrane strains are present as well. Again, MITC9, Q8H and S4 exhibit excellent performance. As expected, the predictions of the S4 and S3 elements are closer than in the previous loading case, and those of the S4R element are in closer agreement with the reference solution. As observed in the previous loading case, the performances of T6 and T6H are satisfactory and comparable to each other.

3.4.2. Very thin beam

In this case, the beam thickness is $h = 0.0032$ m, corresponding to an aspect ratio $L/h = 3750$. For Q8H and MITC9, uniform meshes with one and two elements across the width are used, e.g., 1×8 and 2×8, plus one finer mesh of 4×30, whereas for T6H and T6, 2, 4, 8 and 16 elements are used across the width with balanced meshes. For S4, S4R and S3, the meshes are similar to those used for the thick beam.

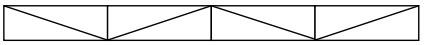

Fig. 13b. Two elements in width mesh, the warping feature is not shown, for clarity.

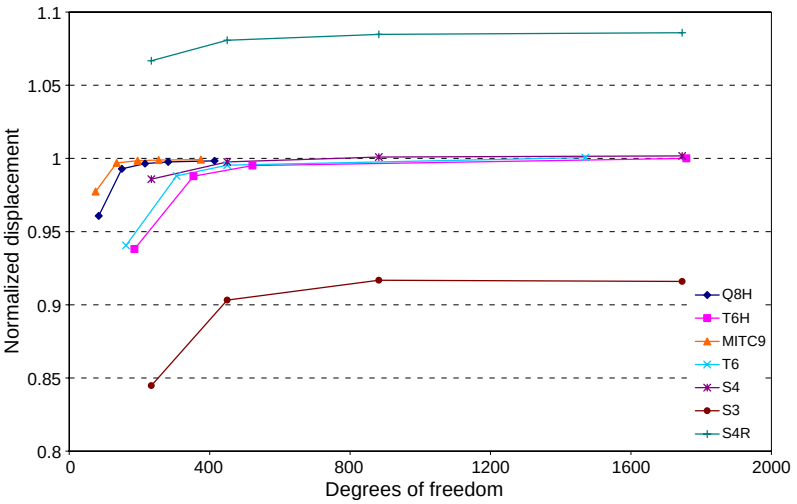

Fig. 14. Displacement U_y of 0.32 m thick beam at point of loading for $P_y = 1$ N.

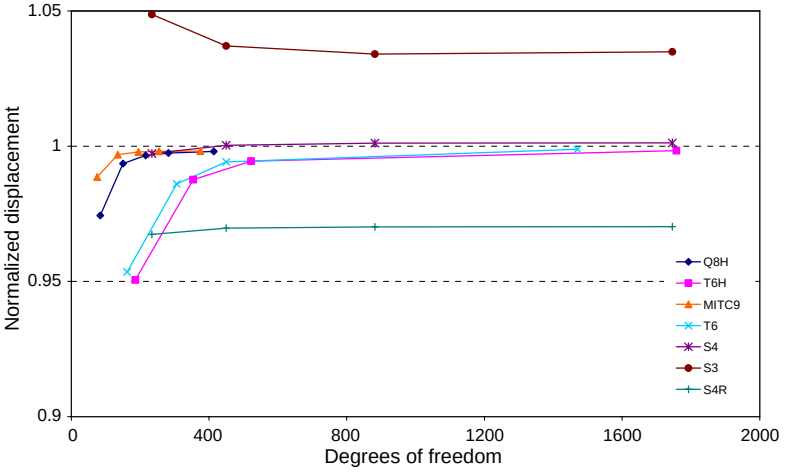

Fig. 15. Displacement U_z of 0.32 m thick beam at point of loading for $P_y = 1$ N.

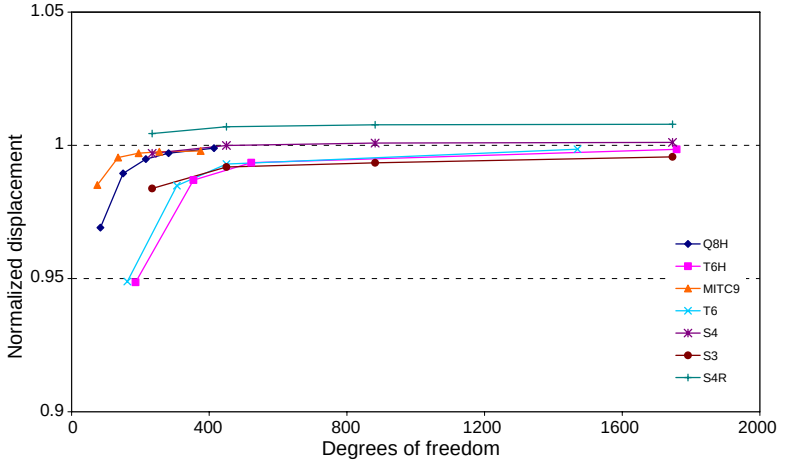

Fig. 16. Displacement U_z of 0.32 m thick beam at point of loading for $P_z = 1$ N.

Predictions are shown in Figs. 17a and 18a for out-of-plane loading; reference solutions from beam theory: $U_y = 1.296$ mm, $U_z = -1.878$ mm. Fig. 19a summarizes the results for in-plane loading; reference solution $U_z = 5.316$ mm. In Figs. 17b,18b and 19b, the same results are presented excluding those of the T6 and T6H elements, to enable comparison of the best performing elements. In view of the very large aspect ratio, shear and membrane locking dominate the element response. Furthermore, the dominant deformation is bending along the beam span for both loading cases, except in the immediate vicinity of the clamped end for the case of out-of-plane loading. For in-plane loading, bending should be nearly inextensible. Excellent performances are still obtained with MITC9 and Q8H elements. For Q8H, the convergence is not completely monotonic for meshes between the 1×12 (414 dofs) and 2×8 (462 dofs) configurations; the latter mesh features more dofs, but the former yields slightly better results, due to a better aspect ratio of the elements. The transition from 1×12 to 2×8 meshes (375 and 424 dofs, respectively) also resulted in a decrease of the prediction accuracy for MITC9. The drop is smaller than that observed for Q8H for the out-of-plane loading P_y (Figs. 17b and 18b), whereas for the in-plane loading P_z, the contrary is observed (Fig. 19b). For the MITC9, convergence is nearly reached with the 2×8 mesh. For this element, also note the convergence "from above" for the component U_z of the out-of-plane loading P_y (Fig. 18a or 18b). The S4R and S3 elements now yield excellent predictions as well. In fact, their predictions are slightly better than those of the S4 element. The

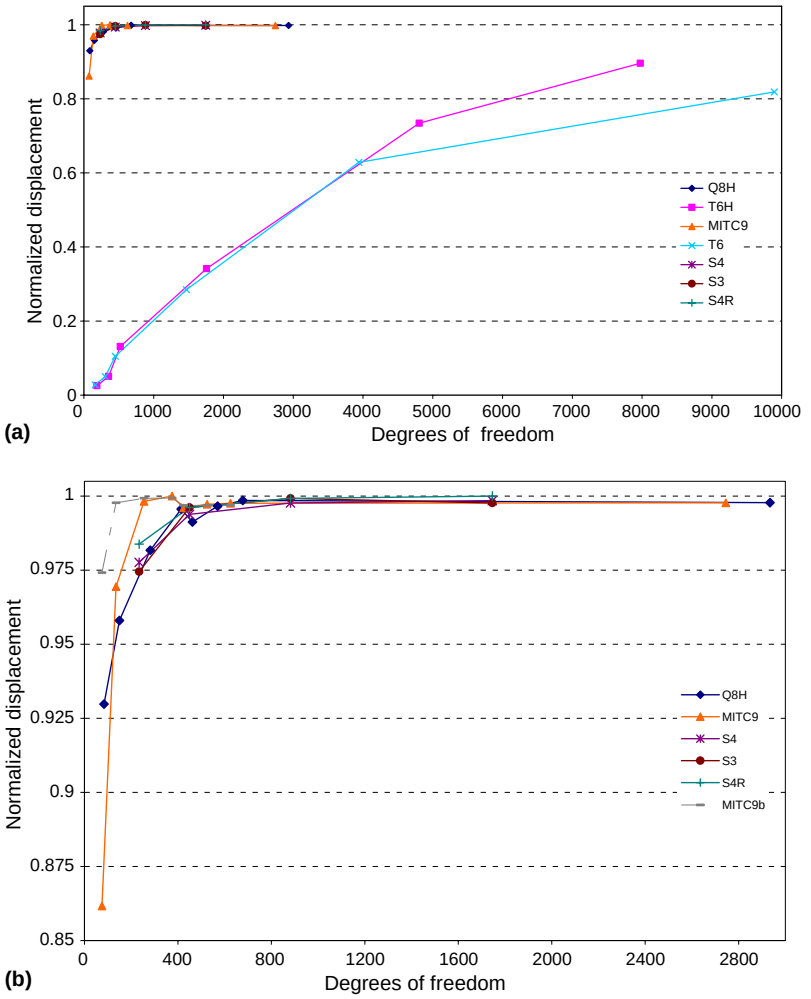

Fig. 17a and 17b. Displacement U_y of 3.2 mm thick beam at point of loading for $P_y = 1e{-}6$ N.

performance of the T6H and T6 elements are the poorest, but interestingly, the former shows a better convergence rate than the latter, which suffers an even more severe locking effect.

In ADINA, shell directors at each node can be input independently. This option is useful when dealing with complex surfaces and using very coarse meshes. Indeed, directors that are normal to the actual shell surface can be input exactly, rather than using directors that are normal to the approximate surface defined by the nodes of the coarse mesh. To illustrate this feature, Table 2 shows the predictions using these two types of directors, when dealing with the 1×2 and 1×4 coarse meshes for the 3.2 mm thick, pre-twisted beam. Clearly, in this case, using approximate directors has little effect on the accuracy of the predictions. A detailed study of the effect of director orientation on the convergence characteristic of shell finite elements is reported by Chapelle and Bathe (2003), Hiller and Bathe (2003); convergence of the MITC9 element is discussed by Bathe et al. (2000).

For the pre-twisted beam, the shell's surface is generated by the motion of a straight line sweeping along the beam's axis while rotating at a constant rate, from 0° to 90°. Two choices are now possible for the directors. In the first case, directors, called *shell directors*, are selected to be normal to the shell's surface. In the second case, since this is a "pre-twisted *beam*" problem, directors, called herein as *beam directors*, are selected to be normal to the beam's cross-section, i.e. they rotate at a constant rate but remain in the plane perpendicular to the beam's axis. New calculations were performed using beam directors as a direct input to ADINA, as assumed in the analytical beam theory used to calculate the reference solution. These new predictions,

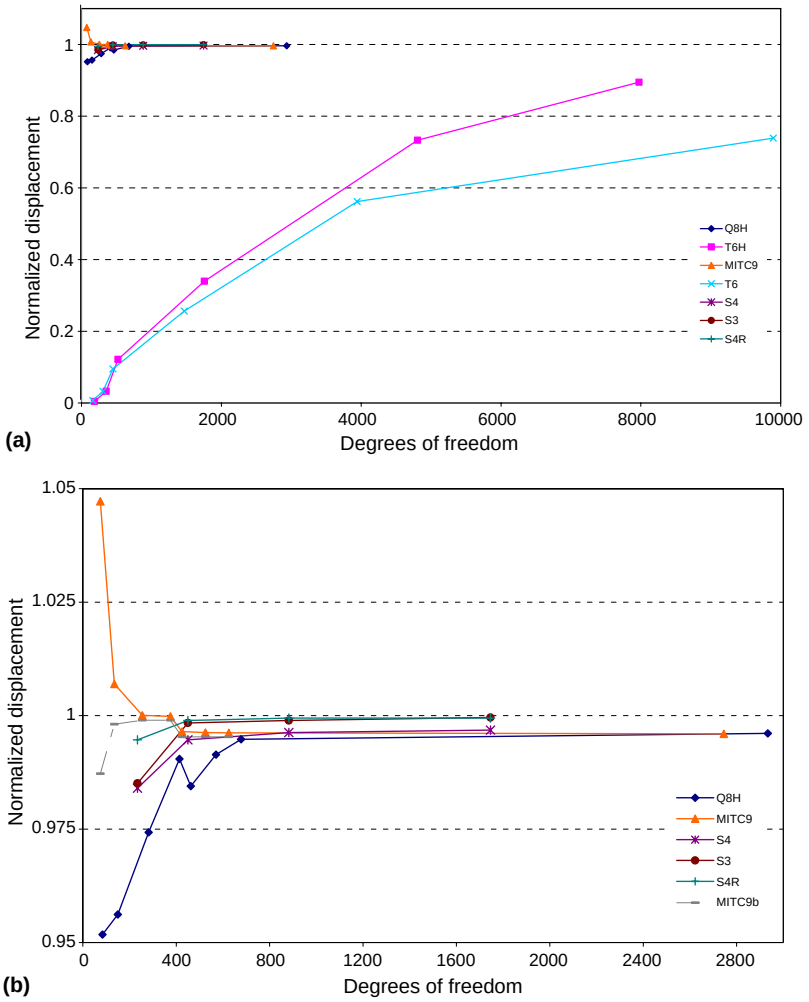

Fig. 18a and 18b. Displacement U_z of 3.2 mm thick beam at point of loading for $P_y = 1$ e−06 N.

labeled as MITC9b in Figs.17b, 18b and 19b, present a marked improvement, especially for the 1×2 mesh. For the in-plane loading P_z case, $U_z = 0.8814$ and 0.9664 for the shell and beam directors, respectively. For finer meshes (from 1×8 onward), both director types yield very similar predictions, as should be expected. In the case of the thick beam, computations performed with the two types of directors showed very little difference.

Finally, it is worth noting that for the very thin beam problem, most of shell elements investigated here, especially MITC9 and Q8H, converge to solutions that are slightly stiffer than the beam theory solutions.

3.5. Morley skew plate under transverse load

The objective of this test is to determine the robustness of the elements to distortion in their geometry. The simple test consists of a skew plate simply supported on all the edges and subjected to a uniform transverse pressure p. The severity of the distortion increases as the skew angle α increases. The tests were carried for two values of α:$\alpha = 60°$ and the more severe case, $\alpha = 30°$. The Morley skew plate mainly tests for the effects of bending of distorted plate/shell elements; shear strains are negligible. The sides L of the plate are of unit length and the plate thickness is $t = 0.01$. The plate material has a Young's modulus of $E = 1$ force per unit area and a Poisson's ratio of $v = 0.3$. The applied load has a magnitude of $p = 1$ force per unit area. Uniform meshes are used for the quadrilateral elements, whereas the meshes used for triangular elements are shown in

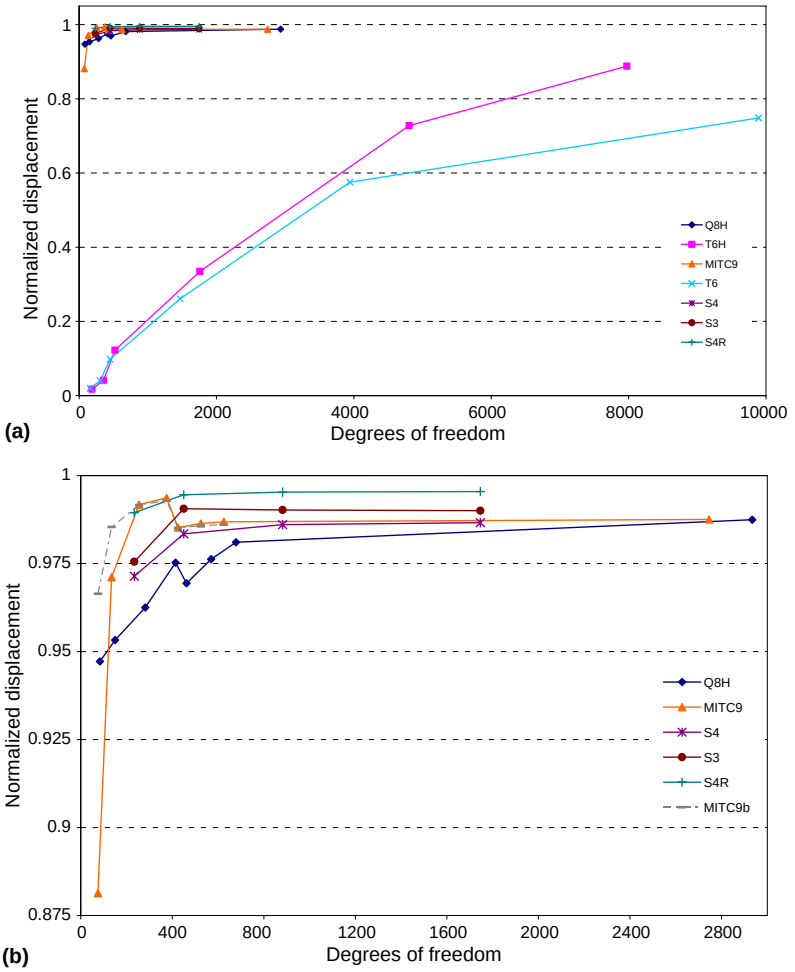

Fig. 19a and 19b. Displacement U_z of 3.2 mm thick beam at point of loading for $P_z = 1e{-}6$ N.

Table 2
Normalized displacements obtained with the approximate and exact directors for the 3.2 mm thick beam

	1×2 mesh		1×4 mesh	
	Approximate directors	Exact directors	Approximate directors	Exact directors
Out-of-plane loading P_y: U_y	0.8616	0.8683	0.9694	0.9692
Out-of-plane loading P_y: U_z	1.0472	1.0555	1.0070	1.0067
In-plane loading P_z: U_z	0.8814	0.8864	0.9711	0.9715

Fig. 20. For this problem, the mesh orientation depicted in Fig. 20 yields better predictions than for a mesh orientation along the other diagonal of the plate or for balanced meshes, as those used in the previous examples. The quantity of interest is the vertical deflection at the centre point C. The reference solution of 2.79552e4 unit length for $\alpha = 60°$ and 4.4553e3 unit length for $\alpha = 30°$ are used to normalize the results.

Since the deformation mostly consists of bending strains with little shearing deformations, the predictions of the *ABAQUS* elements S4, S4R and S3 are similar; the more accurate evaluation of the membrane strain in the S4 element as compared to S4R and S3 is of little importance here.

The predictions for $\alpha = 60°$ are plotted in Fig. 21. The MITC9, S4R, S4 and S3 elements yield excellent predictions with faster convergence rates (especially S3) than those observed for the Q8H element; this latter

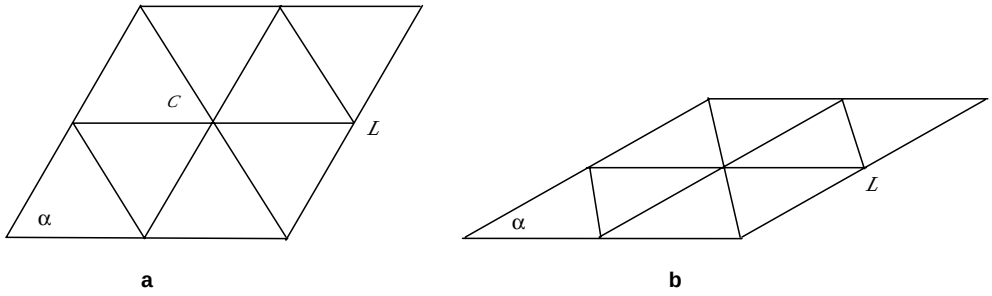

Fig. 20. Morley skew plate test problem – (a) $\alpha = 60°$; (b) $\alpha = 30°$; $L = 1$.

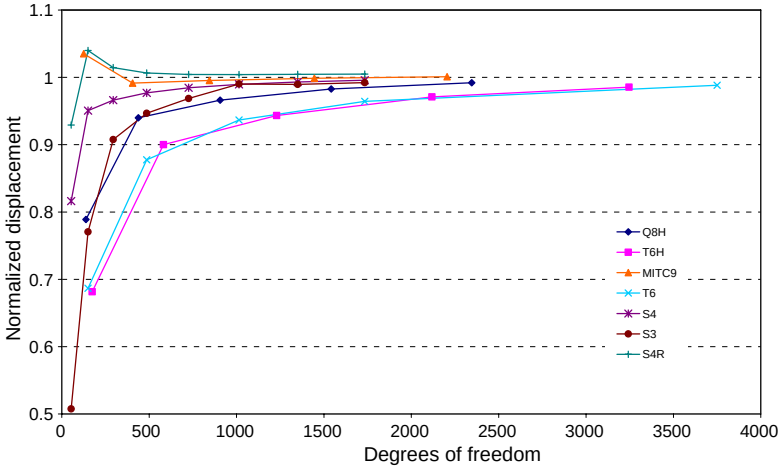

Fig. 21. Displacement of Morley skew plate for $\alpha = 60°$ at center point C.

element, however, converges monotonically to the reference solution at an acceptable rate. Elements T6H and T6 give equivalent results and converge monotonically at an acceptable rate as well.

The predictions for $\alpha = 30°$ are plotted in Fig. 22. Interestingly, the best performances are observed for S4R and S3 elements, while element S4 is hindered by shear locking and exhibits a lower convergence rate.

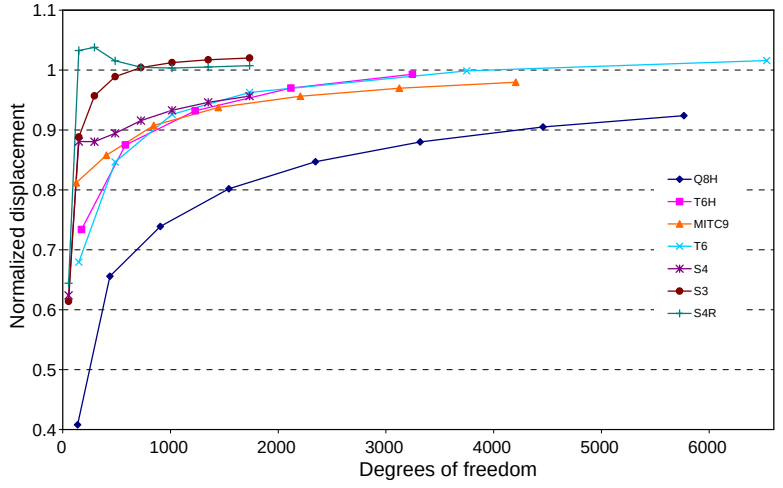

Fig. 22. Displacement of Morley skew plate for $\alpha = 30°$ at center point C.

Elements T6H, T6 and MITC9 show good performance. The results of MITC9 are in excellent agreement with those reported in Bucalem and Bathe (1993). As observed in the previous case, the predictions of the two triangular elements are comparable. The performance of element Q8H is rather poor, showing relatively lower convergence rate due to persisting shear locking, which is clearly more severe than for $\alpha = 60°$. These results confirm the fact that the heterosis element Q8H is quite sensitive to mesh distortion, as observed earlier for plate bending problems, see for instance, Lee and Wong (1982).

3.6. Circular plate under uniform pressure

The deformation of a circular plate is often used to verify results of new plate elements because analytical solutions are readily available in this case. In this test problem, a circular plate clamped around its circumference is subjected to a uniform transverse pressure. The deflection and bending moments at the centre point

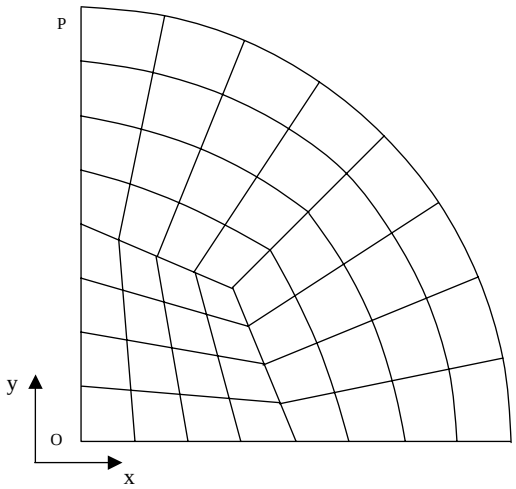

Fig. 23. Mesh used for circular plate problem.

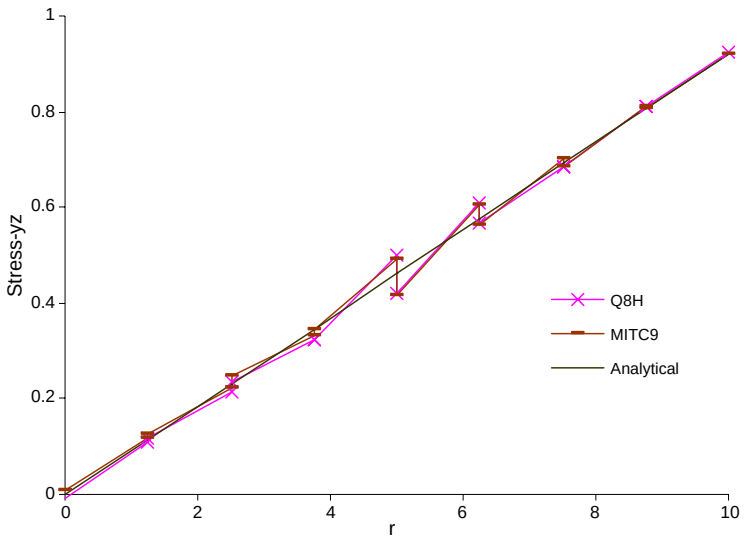

Fig. 24. Transverse shear stress within circular plate.

are normally used to check the accuracy of the elements. This benchmark problem is used here to evaluate the accuracy of transverse shear stress predictions when a classical mesh pattern is used for quadrilateral elements. For a single mesh, the predictions of the Q8H and MITC9 elements are compared to the analytical solution. As with the Morley skewed plates, the circular plate is subject to bending loads with minimal shearing. The plate used in this test has a radius of 10 m and a thickness h of 0.2 m. The material has a Young's modulus of $E = 2.1\ \mathrm{MN/m^2}$ and Poisson's ratio of $v = 0.3$. The pressure load has a magnitude of $p = 0.03072\ \mathrm{N/m^2}$. The classical mesh pattern is shown in Fig. 23; due to symmetry, only a quarter of the plate is modeled.

The analytical solution for the transverse shear stress τ_{yz} based on Mindlin/Reissner theory is plotted along line OP in Fig. 24, together with the predictions of the Q8H and MITC9 elements. The calculated values are at the common nodes of two elements. The transverse shear strain based on Mindlin/Reissner theory is constant through the thickness and so is the stress, due the material homogeneity. The analytical solution for the shear stress along OP is easily found to be $\tau_{yz} = pr/2hk$, where the shear correction factor is $k = 5/6$. Very good predictions are obtained from both MITC9 and Q8H elements when compared to the analytical solution. The results of MITC9 and Q8H are also very close to each other. For both elements, the discontinuities at the junction nodes are within an acceptable range. It is worth noting that the mesh used is not a regular and contains a number of distorted elements. Yet, as shown, excellent results are obtained with Q8H.

4. Conclusions

The following conclusions are drawn based on the numerical experiments conducted in this work:

(1) On the whole, the quadrilateral quadratic heterosis element Q8H based on the selectively reduced integration scheme is very efficient when relatively regular meshes are used. For regular meshes, the performance of element Q8H is comparable to that of quadrilateral element MITC9 although for several test cases studied, the convergence rate of MITC9 is slightly better than that of Q8H. With severely distorted elements, Q8H exhibits low convergence rate, as observed by other researchers.
(2) MITC9 is the highest performance element: it combines accurate results for coarse meshes with insensitivity to element distortions, although it is computationally more expensive than the others as it employs a full integration scheme.
(3) In general, for regular meshes, MITC9 and Q8H outperform the other elements including S4, S4R and S3 (or S3R), especially in the cases where complex deformations are encountered. S4, S4R and S3 are general-purpose shell elements from the commercial software package, *ABAQUS*. The performance of S4 is better than that of S4R and S3 for problems with significant membrane strains. For bending dominated problems with minimum membrane strains, S4R and S3 yield comparable or better predictions. S4 is computationally more expensive than S4R.
(4) Based on the concepts of Q8H, a new element, T6H called quadratic triangular heterosis element has been presented. The interpolation functions of this element include quadratic and cubic polynomials. T6H also uses the selectively reduced integration rule, but it presents no spurious mechanism, while Q8H exhibits one membrane artificial mechanism, which is not communicable. For most problems tested, the performance of T6H is comparable to that of T6, used here as its benchmark. In the case of very thin shells, T6H performs better than T6, which suffers more shear and/or membrane locking than T6H. T6 is the quadratic triangular element from the commercial software package, *ANSYS*.
(5) In general, the performance of T6 and T6H is the poorest among all the elements investigated. But, these two elements are the sole that have shown monotonic convergence characteristic for all the problems studied.

Appendix

The seven interpolation functions of the T6H element for the interpolation of the rotations $\tilde{\theta}_\alpha$ are:

$$N_1^{(2)}(\xi_1,\xi_2) = \xi_2(2\xi_2 - 1) + \frac{1}{9}N_7^{(2)}$$

$$N_2^{(2)}(\xi_1,\xi_2) = (1-\xi_1-\xi_2)[2(1-\xi_1-\xi_2) - 1] + \frac{1}{9}N_7^{(2)}$$

$$N_3^{(2)}(\xi_1,\xi_2) = \xi_1(2\xi_1 - 1) + \frac{1}{9}N_7^{(2)}$$

$$N_4^{(2)}(\xi_1,\xi_2) = 4\xi_2(1-\xi_1-\xi_2) - \frac{4}{9}N_7^{(2)}$$

$$N_5^{(2)}(\xi_1,\xi_2) = 4\xi_1(1-\xi_1-\xi_2) - \frac{4}{9}N_7^{(2)}$$

$$N_6^{(2)}(\xi_1,\xi_2) = 4\xi_1\xi_2 - \frac{4}{9}N_7^{(2)}$$

where $N_7^{(2)}$ is the interpolation function associated to the internal node of the T10 element; $N_7^{(2)}$ is a cubic polynomial,

$$N_7^{(2)}(\xi_1,\xi_2) = 27\xi_1\xi_2(1-\xi_1-\xi)$$

References

ABAQUS, 1998. ABAQUS Theory Manual, ABAQUS/Standard User's Manual, vol. II, Version 5.8.

ADINA, 2005. ADINA System Online Manuals, Version 8.3.

ANSYS, 1998. ANSYS User's Manual, Report Version 5.5.

Bathe, K.J., Dvorkin, E.N., 1986. A formulation of general shell element – the use of mixed interpolation of tensorial components. International Journal for Numerical Methods in Engineering 22, 697–722.

Bathe, K.J., Iosilevich, A., Chapelle, D., 2000. An evaluation of the MITC shell elements. Computers & Structures 75, 1–30.

Batoz, J.L., Lardeur, P., 1989. A discrete shear triangular nine d.o.f. element for the analysis of thick to very thin plates. International Journal for Numerical Methods in Engineering 29, 533–560.

Batoz, J.-L., Dhatt, G., 1990. Modélisation des structures par éléments finis, Hermès édition.

Batoz, J.-L., Katili, I., 1992. On a simple triangular Reissner/Mindlin plate element based on incompatible modes and discrete constraints. International Journal for Numerical Methods in Engineering 35, 1603–1632.

Belytschko, T., Stolarski, H., Liu, W.K., Carpenter, N., Ong, J.S.J., 1985. Stress projection for membrane and shear locking in shell finite elements. Computer Methods in Applied Mechanics and Engineering 51, 221–258.

Bucalem, M.L., Bathe, K.J., 1993. High-order MITC general shell elements. International Journal for Numerical Methods in Engineering 36, 3729–3754.

Carnoy, E., Laschet, G., 1992. *Eléments de coque isoparamétriques*, Université de Liège, Belgium, LTAS, Rapport SF-108, Novembre.

Chapelle, D., Bathe, K.J., 2003. The Finite Element Analysis of Shells – Fundamentals. Springer-Verlag, Berlin.

Hiller, J.F., Bathe, K.J., 2003. Measuring convergence of mixed finite element discretizations: an application to shell structures. Computers & Structures 81, 639–654.

Huang, H.C., Hinton, E., 1986. A new nine node degenerated shell element with enhanced membrane and shear interpolation. International Journal for Numerical Methods in Engineering 22, 73–92.

Hughes, T.J.R., Cohen, M., Haroun, M., 1978. Reduced and selective integration technique in finite element analysis of plates. Nuclear Engineering and Design 46, 202–222.

Hughes, T.J.R., 1987. The Finite Element Method: Linear Static and Dynamic Finite Element Analysis. Prentice-Hall.

Hughes, T.J.R., Cohen, M., 1978. The heterosis finite element for plate bending. Computers and Structures 9, 445–450.

Hughes, T.J.R., Liu, W.K., 1982. Nonlinear finite element analysis of shells: Part I three-dimensional shells. Computer Methods in Applied Mechanics and Engineering 26, 331–362.

Jang, J., Pinsky, P., 1987. An assumed covariant strain based 9-node shell element. International Journal for Numerical Methods in Engineering 24, 2389–2411.

Lee, S.W., Wong, S.C., 1982. Mixed formulation finite elements for Mindlin theory plate bending. International Journal for Numerical Methods in Engineering 18, 1297–1311.

Liu, J., Riggs, H.R., Tessler, A., 2000. A four-node, shear deformable shell element developed via explicit Kirchoff constraints. International Journal for Numerical Methods in Engineering 49, 1065–1086.

Massin, P., Laulusa, A., Mikdad, M.A.L. 2000. Eléments finis de coques volumiques, R3.07.04-A, Code_Aster, HI-75/00/006/A, EDF/MTI/MMN, SAMTECH-France.

McNeal, R.H., 1982. Derivation of element stiffness matrices by assumed strain distribution. Nuclear Engineering and Design 70, 3–12.

McNeal, R.H., Harder, R.L., 1985. A proposed standard set of problems to test finite element accuracy. Finite Elements in Analysis and Design 1, 3–20.

Noor, A.K., 1990. Bibliography of monographs and surveys on shells. Applied Mechanics Review 43 (9), 223–234.

Noor, A.K., Belytschko, T., Simo, J.C. (Eds.), 1989. Analytical and computational models of shells, CED-vol. 3. ASME.

Pugh, E.D., Hinton, E., Zienkiewicz, O.C., 1978. A study of triangular plate bending element with reduced integration. International Journal for Numerical Methods in Engineering 12, 1059–1078.

Reddy, J.N., 1984. A simple higher-order theory for laminated composite plate. Journal of Applied Mechanics 51, 745–752.

Tessler, A., Hughes, T.J.R., 1985. A three-node Mindlin plate element with improved transverse shear. Computer Methods in Applied Mechanics and Engineering 50, 71–101.

Wempner, G., 1990. Mechanics and finite element of shells. Applied Mechanics Review, ASME 42 (5), 129–142.

Zhang, Y.X., Cheung, Y.K., Chen, W.J., 2000. Two refined non-conforming quadrilateral flat shell elements. International Journal for Numerical Methods in Engineering 49, 355–382.

Zienkiewicz, O.C., Taylor, R.L., Too, J.M., 1971. Reduced integration technique in general analysis of plates and shells. IJNME 3, 275–290.

Zienkiewicz, O.C., 1977. The Finite Element Method, third ed. McGraw-Hill.